

Analytical theory of second harmonic generation from a nanowire with noncentrosymmetric geometry

Raksha Singla* and W. Luis Mochán†

Instituto de Ciencias Físicas, Universidad Nacional Autónoma de México, Apartado Postal 48-3, 62251 Cuernavaca, Morelos, Mexico

 (Received 2 January 2019; revised manuscript received 25 February 2019; published 14 March 2019)

We analytically investigate the effect of a noncentrosymmetric geometry in the optical second harmonic (SH) generation from a nanowire made of a centrosymmetric material, in the interior of which quadratic optical processes are suppressed. We consider an infinite cylinder with a cross section that is slightly deformed away from a circle and with a radius much smaller than the wavelength. We calculate the induced linear and nonlinear fields perturbatively in terms of the deformation parameter, and we obtain the nonlinear dipolar and quadrupolar hyperpolarizabilities, whose spectra we evaluate for metallic and dielectric materials. We show that for very small deformations, the dipolar contribution to the response competes with the quadrupolar term, and may even be dominant. We explore the spectra of the hyperpolarizability and identify the contributions to its structure for metallic and dielectric nanowires. We also discuss the nature of the SH radiation at various frequencies, and we find that it may be dominated by the dipolar or the quadrupolar term, or that both may compete yielding nonsymmetric radiation patterns. Our calculation may be employed to assess, calibrate, and test numerical SH calculations.

DOI: [10.1103/PhysRevB.99.125418](https://doi.org/10.1103/PhysRevB.99.125418)

I. INTRODUCTION

In recent years, the availability of novel techniques to produce nanoparticles with different shapes has attracted much attention as they can be engineered to exhibit unique nonlinear optical properties that are sensitive to their environment as well as their morphologies [1,2]. Exploring second harmonic generation (SHG) from nanoparticles and nanostructures has proven to be an extraordinary tool to probe the properties of their surfaces and interfaces. The surface sensitivity of the SH signal is due to the fact that the bulk signal is strongly suppressed within centrosymmetric systems; within the electric dipolar approximation, SHG from a centrosymmetric system takes place only at the surface as the bulk contribution is forbidden due to symmetry. The surface would also be expected to dominate the SHG from nanoparticles made of centrosymmetric materials, but if they possess a centrosymmetric shape there would be a cancellation of the surface contributions to the nonlinear electrical dipole moment arising from opposite sides, leaving only quadrupolar and higher moments. However, when subjected to a nonuniform polarizing field, a symmetrical particle can generate SH due to the contributions arising from the excitation of a nonlocal dipole moment [3–5]. On the other hand, a homogeneous external field would generate a nonvanishing dipolar SH response even from nanoparticles made of centrosymmetric material if their geometry is noncentrosymmetric. SHG from nanoparticles, arrays of nanoparticles, and nanostructured materials with a variety of geometries have been demonstrated experimentally and with supporting numerical [6–10] investigations.

Recently, by performing experiments on arrays of differently shaped nanoparticles [11] it was shown that the effect of a noncentrosymmetric geometry supersedes that of the local field enhancement for the efficient generation of a SH signal. These experiments illustrate that the polarization of light and the noncentrosymmetric geometry play important roles in the efficiency of the SHG as the overall SH response as well as the plasmonic resonance is also governed by the distribution of the linear and SH near fields. The results have been qualitatively explained through numerical computations of the SH near fields. However, in these calculations only one component of the nonlinear surface susceptibility tensor was considered, and it was taken as an adjustable parameter. Several theoretical models have been proposed to study SH scattering in the Rayleigh limit from small symmetrical nanoparticles [12] and from particles of arbitrary size [13–17] to include the effects of retardation and to explore SHG within the framework of Mie theory. An implementation of the discrete dipole approximation (DDA) model to explore SHG from small nanoparticles of various kinds was employed to study the influence of their shapes and sizes on their nonlinear optical properties [18]. Different studies involving various numerical computation techniques applied to diverse geometries have since then been reported. Some of them used the finite-difference time-domain (FDTD) method to investigate the SHG from nanoholes within a metal film [10], and in particular, from an array of E-shaped nanoholes [9]. Others explored the effect of deformations of metallic spheres [19] on SHG using the finite-element method (FEM). Investigation of SHG from gold split ring resonators [20] used different theoretical models and compared their applicability. A surface integral approach was used to evaluate SH scattering from periodic metallic-dielectric nanostructures [21], noble metal nanoparticles of arbitrary shape [22,23], and gold nanorods

*raksharuia@icf.unam.mx

†mochan@icf.unam.mx

and nanospheres [24]. Another work reported a numerical computation to explore SHG from a single metallic cylinder, a one-dimensional (1D) chain, and a periodic or a random 2D array of them based on a multiple scattering matrix (MSM) algorithm [25]. Recently, a recursive method was employed to study the SH susceptibility, the tuning of the resonant structures, and the corresponding nonlinear polarization of metamaterials made of an array of asymmetric cross-shaped holes within metallic hosts [26]. Valencia *et al.* [16] computed and compared numerically the SH response of infinite cylinders of various cross sections. In another work [17], the same group performed an analytical calculation of SH radiated fields from an infinite circular cylinder within the framework of Mie theory. However, in both of these works the nonlinear susceptibilities of the material from which cylinders were made and its surface response were not calculated but introduced as free parameters. Furthermore, their treatment of the nonlinear polarization lacks self-consistency, as the linear response to the SH field was neglected.

As illustrated by the studies mentioned above, most of the efforts to investigate SHG from nanostructures have employed experimental or *numerical* methods. To the best of our knowledge, there have been no reports of an *analytical* calculation to study the SH response of nanostructures with a noncentrosymmetric geometry. The purpose of this paper is the calculation of the second-order nonlinear response of an isolated nanowire made up of a centrosymmetric material with small deviations from a symmetrical geometry subjected to a homogeneous external field, obtaining and evaluating analytical expressions for the nonlinear dipolar and quadrupolar hyperpolarizabilities. We restrict our study to small deformations, which allows us to employ a perturbative scheme in order to be able to solve the field equations analytically for linear and SH induced fields within and beyond the surface of the nanowire. We consider the simplest geometry for which there is no centrosymmetry, namely a cylinder having a slightly deformed, near-circular cross section with a threefold symmetry, and we use a nonretarded approximation to obtain the near fields, which we use afterward to calculate the electromagnetic fields in the radiation zone. We discuss the resonant structure of the nonlinear response for a model metal and a dielectric nanowire, the relation between the different components of the response tensor due to the symmetry in the system, and we study the angular radiation patterns of the nanowire and their evolution as the frequency sweeps across the various resonances. As expected, we find the dipolar response to be highly dependent on the deformation parameter. Furthermore, a deviation of only 1% away from the symmetry of the shape of the nanowire results in a strong competition with the quadrupolar response for very small cross sections.

The structure of the paper is the following. In Sec. II, we describe our theory to investigate analytically SHG from a deformed infinite cylinder, obtaining expressions for the nonlinear dipolar and quadrupolar hyperpolarizabilities (Sec. II A) and the SH radiation patterns (Sec. II B). Section III illustrates our results for deformed cylinders made up of a Drude metal and a resonant dielectric. Finally, we present our conclusions in Sec. IV.

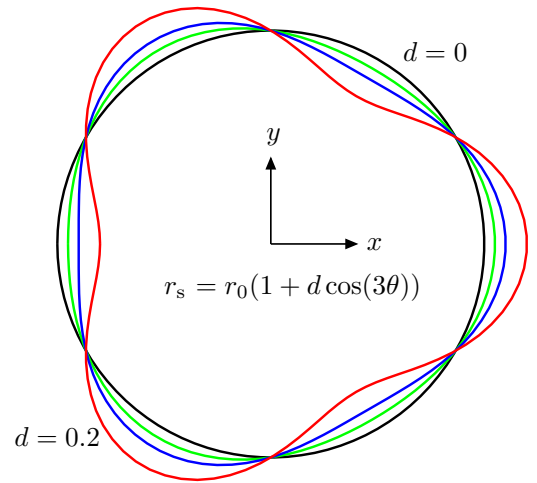


FIG. 1. Cross section of a deformed cylinder described by Eq. (1) for various values of the deformation parameter $d = 0.0, \dots, 0.2$.

II. NONLINEAR RESPONSE OF A DEFORMED CYLINDER

A. Second-order hyperpolarizabilities

We consider an isolated, infinitely long cylinder placed in vacuum with its axis along the \hat{z} direction and a slightly deformed cross section defined in polar (r, θ) coordinates as

$$r_s(\theta) = r_0(1 + d \cos 3\theta) \quad (1)$$

(see Fig. 1), where r_0 is the radius of a symmetric nominal circular cylinder and d is a small deformation parameter. We remark that we chose this geometry as it is the most simple one that lacks inversion geometry. Also note that our system possesses a mirror ($y \rightarrow -y$) and a 120° rotational symmetry. We will study the nonlinear dipolar \mathbf{p} and quadrupolar \mathbf{Q} moments induced per unit length along the axis of the cylinder. We subject the particle to a homogeneous external electric \mathbf{E}^{ex} field oscillating at frequency ω . Due to the overall noncentrosymmetry of the geometry of the particle, \mathbf{p} is expected to have a local contribution proportional to $\mathbf{E}^{\text{ex}}\mathbf{E}^{\text{ex}}$, which we write as

$$p_i = \gamma_{ijk}^d E_j^{\text{ex}} E_k^{\text{ex}}, \quad (2)$$

where γ_{ijk}^d is the dipolar hyperpolarizability, and we use Einstein summation convention. Similarly, the induced quadratic 2D quadrupole moment, defined as

$$Q_{ij} = \int d^2r \rho(\mathbf{r})(2r_i r_j - r^2 \delta_{ij}) \quad (3)$$

(notice the difference with the usual 3D definition), is given by

$$Q_{ij} = \gamma_{ijkl}^Q E_k^{\text{ex}} E_l^{\text{ex}}, \quad (4)$$

where γ_{ijkl}^Q is the quadrupolar hyperpolarizability. Here, $\rho(\mathbf{r})$ is the 2D charge density.

For simplicity, we first assume that the external field is polarized along the \hat{x} direction, $\mathbf{E}^{\text{ex}} = E_0 \hat{x}$. Given the direction of the external field and the symmetries in the system, the only nonzero component of the nonlinear dipole moment induced

in this case is p_x , which we write as

$$p_x = \gamma^d E_0^2 \quad (5)$$

in terms of a dipolar nonlinear response γ^d , which is simply related to all the components of the full dipolar hyperpolarizability γ_{ijk}^d . In this case, the nonlinear quadrupole moment has only two nonzero components

$$Q_{xx} = -Q_{yy} = \gamma^Q E_0^2, \quad (6)$$

which we write in terms of a nonlinear response γ^Q , related to the full quadrupolar hyperpolarizability γ_{ijkl}^Q . In this section, we calculate analytically γ^d and γ^Q .

In the nonretarded regime, the linear self-consistent near field may be obtained by solving Laplace's equation beyond and within the particle and applying boundary conditions at its interface. We start with the general solution of Laplace's equation outside

$$\phi_1^{\text{out}} = \phi^{\text{ex}} + \sum_{l=0}^{\infty} r^{-l} (s_l \cos l\theta + t_l \sin l\theta) \quad (7)$$

and within

$$\phi_1^{\text{in}} = \sum_{l=0}^{\infty} r^l (u_l \cos l\theta + v_l \sin l\theta) \quad (8)$$

the particle, with multipolar coefficients s_l , t_l , u_l , and v_l , which we expand as power series on the deformation parameter d ,

$$\beta_l = \sum_{n=0}^{\infty} \beta_l^{(n)} d^n, \quad (9)$$

where $\phi^{\text{ex}} = -E_0 r \cos \theta$ is the external scalar potential, and the generic coefficients β_l stand for any of s_l , t_l , u_l , or v_l . To perform analytical calculations, we will restrict ourselves to small deformations and consider terms up to linear order in d only. Thus, solving Laplace's equation with appropriate boundary conditions [27] at the origin, the surface of the particle, and infinity, we obtain the self-consistent linear potential

$$\frac{\phi_1^{\text{out}}}{E_0} = r \cos \theta - \frac{1 - \epsilon_1}{1 + \epsilon_1} \frac{r_0^2}{r} \cos \theta - d \left[\left(\frac{1 - \epsilon_1}{1 + \epsilon_1} \right)^2 \frac{r_0^3}{r^2} \cos 2\theta + \frac{1 - \epsilon_1}{1 + \epsilon_1} \frac{r_0^5}{r^4} \cos 4\theta \right], \quad (10)$$

$$\frac{\phi_1^{\text{in}}}{E_0} = \frac{2}{1 + \epsilon_1} r \cos \theta + 2d \frac{1 - \epsilon_1}{(1 + \epsilon_1)^2} \frac{r_0}{r^2} \cos 2\theta, \quad (11)$$

where $\epsilon_g = \epsilon(g\omega)$ is the dielectric response of the particle at the g th harmonic frequency, $g = 1, 2$. From these results, we may obtain the linear electric field \mathbf{E}_1 .

The spatial variation of the self-consistent field within the particle induces a nonlinear polarization [27]

$$\mathbf{P}^{\text{nl}} = n\mathbf{p}^{\text{nl}} - \frac{1}{2}n\nabla \cdot \mathbf{q}^{\text{nl}}, \quad (12)$$

which includes contributions from the nonlinear dipole \mathbf{p}^{nl} and quadrupole \mathbf{q}^{nl} moments of each microscopic polarizable entity within the material, whose number density is n . Note that \mathbf{q}^{nl} may have a finite trace. Using the *dipolium* model [28],

we write

$$\mathbf{p}^{\text{nl}} = -\frac{1}{2e} \alpha_1 \alpha_2 \nabla E_1^2 \quad (13)$$

and

$$\mathbf{q}^{\text{nl}} = -\frac{1}{e} \alpha_1^2 \mathbf{E}_1 \mathbf{E}_1 \quad (14)$$

in terms of the linear electric field and the linear polarizability $\alpha_g \equiv \alpha(g\omega)$ evaluated at the fundamental ($g = 1$) and SH ($g = 2$) frequencies, related to the dielectric function through $\epsilon_g = 1 + 4\pi n\alpha_g$.

The polarization, Eq. (12), yields a nonlinear bulk charge density given by

$$\rho^{\text{nl}} = -\nabla \cdot \mathbf{P}^{\text{nl}}, \quad (15)$$

which evaluates to zero up to linear order in d (it would be nonzero at order d^2). The termination of the nonlinear polarization at the surface of the particle induces a nonlinear surface charge with density $\sigma^b = \mathbf{P}^{\text{nl}}(r_s^-) \cdot \hat{\mathbf{n}}$, where $\hat{\mathbf{n}}$ is a normalized outgoing vector perpendicular to the surface and $r_s^- = r_s^-(\theta)$ denotes a position at the surface just inside the particle. We employ the superindex b to denote the bulk origin of this surface charge. Using Eqs. (10)–(14), we identify

$$\sigma^b = 4d \frac{n}{er_0} \frac{(1 - \epsilon_1)}{(1 + \epsilon_1)^3} \alpha_1 (2\alpha_2 - \alpha_1) \cos \theta E_0^2. \quad (16)$$

As the inversion symmetry of the material is locally lost in a thin selvedge region around the surface, there is a nonlinear polarization induced at the surface of the particle, which we write as

$$P_i^s = \chi_{ijk}^s F_j F_k, \quad (17)$$

where χ_{ijk}^s are the components of the local nonlinear surface susceptibility, and the field \mathbf{F} is defined in terms of quantities that are continuous across the surface to avoid the ambiguity about the position in the selvedge where the fields are to be calculated; \mathbf{F} is made up of the normal projection of the displacement field and the parallel projection of the electric field evaluated at the surface $r_s(\theta)$. Thus,

$$\mathbf{F}(r_s) = \mathbf{E}_1(r_s^+) = \epsilon_1 \mathbf{E}_1^\perp(r_s^-) + \mathbf{E}_1^\parallel(r_s^-), \quad (18)$$

where $\mathbf{E}(r_s^-) = -\nabla \phi^{\text{in}}(r_s)$ and $\mathbf{E}(r_s^+) = -\nabla \phi^{\text{out}}(r_s^+)$, and \perp and \parallel denote the projections normal and parallel to the surface.

We will assume that the thickness of the selvedge region is much smaller than the radius of the cylinder, and thus that the surface can be considered as locally flat. We will further assume *local* invariance under rotations around the surface normal. Hence, the surface susceptibility may be parametrized as

$$\chi_{ijk}^s = \frac{(\epsilon_1 - 1)^2}{64\pi^2 ne} \left(\delta_{i\perp} \delta_{j\perp} \delta_{k\perp} \frac{a}{\epsilon_1^2} + [(1 - \delta_{i\perp})(1 - \delta_{j\perp})\delta_{k\perp} + (1 - \delta_{i\perp})\delta_{j\perp}(1 - \delta_{k\perp})] \frac{b}{\epsilon_1} + \delta_{i\perp}(1 - \delta_{j\perp})(1 - \delta_{k\perp})f \right), \quad (19)$$

in a local reference frame where one of the Cartesian directions is perpendicular and the others are parallel to the

surface. Here, a , b , and f are dimensionless functions of ω used to parametrize the response of the surface [29] given in the *dipolium* model [28] by

$$a(\omega) = 2 \frac{(\epsilon_2 - \epsilon_1)(2\epsilon_1 - \epsilon_2 - \epsilon_1\epsilon_2) + \epsilon_1^2(1 - \epsilon_2) \log(\epsilon_1/\epsilon_2)}{(\epsilon_2 - \epsilon_1)^2}, \quad (20)$$

$$b = -1, \quad (21)$$

$$f = 0. \quad (22)$$

The normal component of the nonlinear polarization induced on the surface of the cylinder is obtained by substituting Eqs. (18) and (19) in Eq. (17),

$$P_{\perp}^s = \frac{1}{32\pi^2 ne} \left(\frac{1 - \epsilon_1}{1 + \epsilon_1} \right)^2 \left\{ (a + f) + (a - f) \cos 2\theta - d \left[4 \frac{1 - \epsilon_1}{1 + \epsilon_1} + 3(a - f) \right] \cos \theta + 4 \frac{1 - \epsilon_1}{1 + \epsilon_1} \cos 3\theta - 3(a - f) \cos 5\theta \right\} E_0^2. \quad (23)$$

The variation of the tangential component of the nonlinear surface polarization along the surface yields another contribution to the surface charge σ^s beyond that due to the termination of the bulk nonlinear polarization σ^b , where we use the superscript s to denote its surface origin. It is given by

$$\sigma^s = -\nabla_{\parallel} \cdot \mathbf{P}_{\parallel}^s, \quad (24)$$

where ∇_{\parallel} is the gradient operator projected along the surface, and \mathbf{P}_{\parallel}^s is the projection of \mathbf{P}^s along the surface. Substituting Eqs. (17) and (19) in Eq. (24), we obtain

$$\sigma^s = \frac{b}{8\pi^2 ner_0} \left(\frac{1 - \epsilon_1}{1 + \epsilon_1} \right)^2 \left[\cos 2\theta + d \left(\cos \theta - 6 \frac{1 - \epsilon_1}{1 + \epsilon_1} \cos 3\theta + 7 \cos 5\theta \right) \right] E_0^2. \quad (25)$$

The screened scalar potential ϕ_2 induced at the SH frequency has $\rho^{\text{nl}} (= 0)$ as an *external* bulk source and the total nonlinear charges induced at the surface, σ^b and σ^s , as external surface sources, together with the normal polarization P_{\perp}^s , which are accounted for through the boundary conditions. The external sources have to be screened by the linear response of the particle at SH frequency ϵ_2 . Thus the equation to be solved for the quadratic scalar potential is

$$\nabla^2 \phi_2 = \begin{cases} 0 & \text{(outside),} \\ -4\pi \rho^{\text{nl}}/\epsilon_2 = 0 & \text{(inside)} \end{cases} \quad (26)$$

subject to the boundary conditions

$$\hat{\mathbf{n}} \cdot \nabla \phi_2(r_s^+) - \epsilon_2 \hat{\mathbf{n}} \cdot \nabla \phi_2(r_s^-) = -4\pi(\sigma^b + \sigma^s), \quad (27)$$

$$\phi_2(r_s^+) - \phi_2(r_s^-) = 4\pi P_{\perp}^s. \quad (28)$$

Equation (27) is the discontinuity of the normal component of the displacement field due to the presence of the nonlinear surface charge. Equation (28) is the discontinuity of the scalar potential due to the presence of the normal nonlinear surface

polarization P_{\perp}^s , which is a dipole layer across the selvedge of the particle. Solving Laplace's equation perturbatively to obtain the self-consistent scalar potential at the SH frequency with terms up to linear order in d , we obtain on the outside

$$\begin{aligned} \frac{\phi_2^{\text{out}}}{E_0^2} = & \frac{d}{4\pi ne} \frac{(1 - \epsilon_1)^2}{(1 + \epsilon_2)(1 + \epsilon_1)^2} \left(4 \frac{\epsilon_1 - 2\epsilon_2 + 1}{1 + \epsilon_1} \right. \\ & + 2b \frac{1 + 3\epsilon_2}{1 + \epsilon_2} + \frac{\epsilon_2(\epsilon_2 - 3)(a - f)}{2(1 + \epsilon_2)} \\ & + \left. \frac{\epsilon_2(7\epsilon_1 - 1)f + (\epsilon_1 - 7)a}{2(1 + \epsilon_1)} \right) \frac{r_0}{r} \cos \theta \\ & + \frac{1}{8\pi ne} \left(\frac{1 - \epsilon_1}{1 + \epsilon_1} \right)^2 \frac{\epsilon_2(a - f) + 2b}{1 + \epsilon_2} \frac{r_0^2}{r^2} \cos 2\theta + \dots, \end{aligned} \quad (29)$$

where we only kept the dipolar and quadrupolar contributions, and we neglected higher multipoles, all of which are at least of order d , as their contribution to the radiation fields would be insignificant for small particles, at least by a factor of order r_0/λ , with λ the wavelength.

Finally, we compare Eq. (29) to the general expression of the 2D scalar potential in polar coordinates, we identify the corresponding components of the multipolar moments, and from Eqs. (5) and (6) we obtain the dipolar

$$\begin{aligned} \gamma^d = & \frac{dr_0}{4\pi ne} \frac{(1 - \epsilon_1)^2}{(1 + \epsilon_2)(1 + \epsilon_1)^2} \left(4 \frac{\epsilon_1 - 2\epsilon_2 + 1}{1 + \epsilon_1} \right. \\ & + 2b \frac{1 + 3\epsilon_2}{1 + \epsilon_2} + \frac{\epsilon_2(\epsilon_2 - 3)(a - f)}{2(1 + \epsilon_2)} \\ & + \left. \frac{\epsilon_2(7\epsilon_1 - 1)f + (\epsilon_1 - 7)a}{2(1 + \epsilon_1)} \right) \end{aligned} \quad (30)$$

and quadrupolar

$$\gamma^Q = \frac{r_0^2}{8\pi ne} \left(\frac{1 - \epsilon_1}{1 + \epsilon_1} \right)^2 \frac{\epsilon_2(a - f) + 2b}{1 + \epsilon_2} \quad (31)$$

nonlinear response functions.

To the lowest order in the deformation parameter, γ^d is proportional to d , and thus, as expected, the dipolar response would disappear for a centrosymmetric circular cross section. On the other hand, γ^Q is independent of d with no contribution proportional to d . Thus, it equals the result for a centrosymmetric circular cylinder with $d = 0$, and therefore is the nonlinear response for a symmetric circular cylinder. An analytical calculation in the retarded regime of the fields radiated at the SH frequency by an infinite circular cylinder can be found in the work by Valencia *et al.* [17]. However, their results cannot be directly compared with Eq. (31) as their calculation was performed for a radius comparable with the wavelength, they took the nonlinear bulk and surface response as parameters, and their calculation is not self-consistent in the SH frequency. From Eqs. (30) and (31) we can identify the contributions arising from the bulk and the surface to the nonlinear hyperpolarizabilities, as the latter are proportional to the surface parameters a , b , and f . Thus, γ^d has both surface and bulk contributions, while γ^Q has only surface contributions. Both γ^d and γ^Q inherit the spectral structure of the surface parameters, namely of $a(\omega)$, and they also

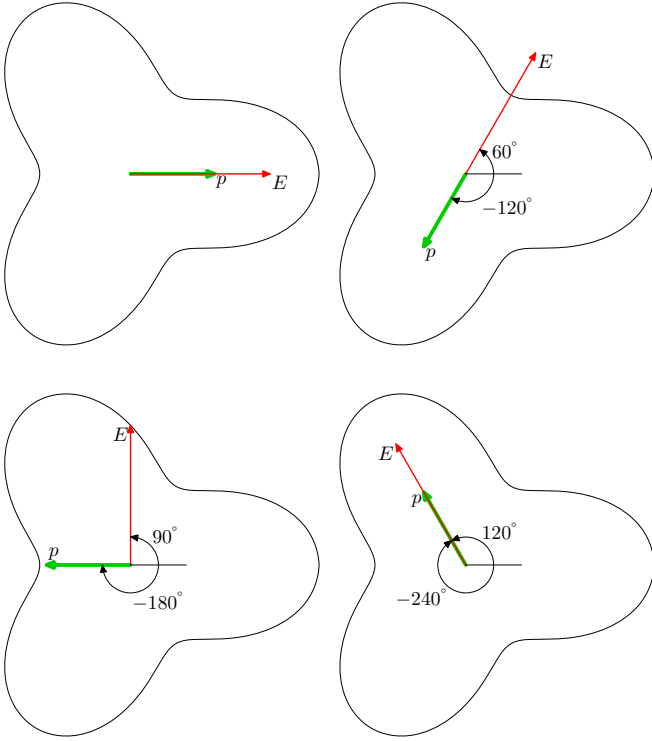


FIG. 2. Direction of the quadratic dipole moment induced in a deformed cylinder by an external field with different directions with respect to the horizontal. As the field rotates clockwise by an angle θ , the dipole rotates counterclockwise by 2θ .

exhibit additional resonances corresponding to the excitation of surface plasmons or surface plasmon-polaritons at the fundamental and second harmonic frequencies, given by $\epsilon_1 = -1$ and $\epsilon_2 = -1$, respectively.

Above we have explicitly shown the calculation of the nonlinear response of the particle with the external field in the \hat{x} direction. One can similarly evaluate the response of the particle to the external field pointing in other directions. However, due to the mirror and the 120° rotation symmetry in our system, all the in-plane components of the dipolar hyperpolarizability are zero except for $\gamma_{xyy}^d = \gamma_{yyx}^d = \gamma_{yxx}^d = -\gamma_{xxx}^d = -\gamma^d$. We have verified these results by repeating the calculations above for external fields pointing along different directions. It turns out that given these symmetry-related relations, the nonlinear dipole moment induced in the deformed cylinder rotates anticlockwise by an angle 2θ when the external electric field is rotated clockwise by θ (see Fig. 2). The symmetry in our system leads to an isotropic quadrupolar response given by $Q_{ij} = \gamma^Q(2E_i E_j - E^2 \delta_{ij})$, the quadratic quadrupolar moment has a principal axis along the external field, and the only non-null components of the quadrupolar hyperpolarizability are $\gamma_{xxx}^Q = -\gamma_{xyy}^Q = -\gamma_{yyx}^Q = \gamma_{yyy}^Q = \gamma^Q$ and $\gamma_{xyx}^Q = \gamma_{yxy}^Q = \gamma_{yxx}^Q = \gamma_{xyy}^Q = 2\gamma^Q$. Thus, for this system our calculations of γ^d and γ^Q using an external field along \hat{x} are sufficient to obtain the full response of the particle. We remark that the shape of the radiation pattern and the total efficiency depend on the polarization of the incident light. This has previously been demonstrated in the work of Czaplicki *et al.* [11]. Their T-shaped particles are

somewhat similar to the ones we have considered, but with a large deformation and without the $2\pi/3$ rotational symmetry. The hyperpolarizability tensor χ_{ijk} of both would have the same set of nonzero components, due to a mirror symmetry, but the lack of rotational symmetry of the T shapes introduces more independent components and a richer resonant structure. The differences are more pronounced for their L-shaped particles. This results in a very different SH local field distribution around the particles and a stronger dependence on the polarization of the incident field. The existence of an inversion symmetry $y \rightarrow -y$ and $2\pi/3$ rotational symmetry also ensures that no nonlinear magnetic dipole is induced in our nanowire in the nonretarded regime. Hence, it is not included in our work. However, we remark that as the particle size increases, retardation effects become important, and the different nonlinear response terms require the incorporation of the gradient of the field leading to nonlocal contributions to the dipolar and quadrupolar response. A nonzero nonlinear magnetic dipole may also be induced. For large particles, the magnetic contribution to the SH response may prove to be dominant over others. This has been demonstrated in the work by Klein *et al.* [30], where SHG from different metamaterials formed of arrays of split ring resonators (SRRs), T-shaped inclusions, and straight wire fragments was measured, and it was found that the SHG for the SRR structure was largely dominated by the magnetic dipole resonance, but not for the straight wire fragments nor the T-shaped structures.

B. SH radiation

Now we turn our attention toward the calculation of the SH angular radiation pattern. Following a procedure similar to the 3D case, one can write down the expressions for the radiated electromagnetic fields in 2D due to localized distributions of charges and currents. Using the vector potential from Eqs. (A7) and (A9) (see the Appendix), we calculate the radiated electromagnetic fields,

$$\mathbf{B} = (1 + i)k^{3/2} \left((\hat{\mathbf{r}} \times \mathbf{p}) - \frac{i}{4}k[\hat{\mathbf{r}} \times (\mathbf{Q} \cdot \hat{\mathbf{r}})] \right) e^{ikr} \sqrt{\frac{\pi}{r}}, \quad (32)$$

$$\mathbf{E} = \mathbf{B} \times \hat{\mathbf{r}}, \quad (33)$$

where k is the wave number and $\hat{\mathbf{r}}$ is the unit vector in the direction of observation. The time-averaged power radiated per unit angle θ due to these radiated fields is

$$\frac{dP}{d\theta} = \frac{rc}{8\pi} \text{Re}[\mathbf{E} \times \mathbf{B}^*] \cdot \hat{\mathbf{r}}. \quad (34)$$

From Eqs. (30) to (34) we obtain

$$\begin{aligned} \frac{dP}{d\theta} = & \frac{cE_0^4 k^3}{16} (4|\gamma^d|^2 \sin^2 \theta - 4k \text{Im}(\gamma^d \gamma^{Q*}) \sin^2 \theta \cos \theta \\ & + k^2 |\gamma^Q|^2 \sin^2 \theta \cos^2 \theta). \end{aligned} \quad (35)$$

The first and last terms correspond to dipolar and quadrupolar radiation, while the middle term corresponds to their interference.

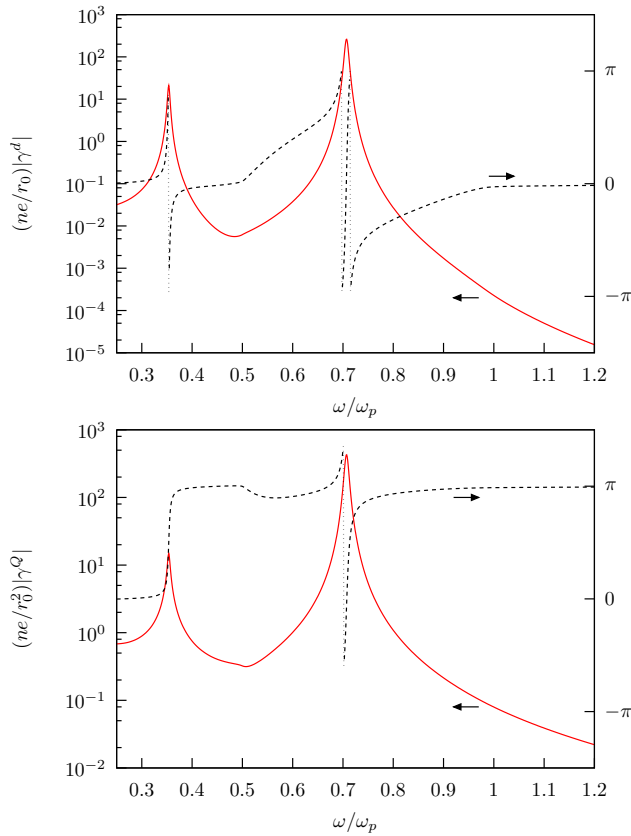


FIG. 3. Normalized absolute value (solid) and phase (dashed) of the dipolar (upper panel) and quadrupolar (lower panel) nonlinear response functions γ^d and γ^Q for a cylinder with deformation parameter $d = 0.01$ made of a Drude metal as a function of the normalized frequency ω/ω_p . The irrelevant abrupt 2π phase jumps are indicated with dotted vertical lines.

III. RESULTS

We consider a particle made up of a Drude metal characterized by its bulk plasma frequency ω_p and electronic relaxation time τ , with dielectric function [31] $\epsilon(\omega) = 1 - \omega_p^2/(\omega^2 + i\omega/\tau)$, with size $r_0 = c/4\omega_p$, with a small deformation parameter $d = 0.01$ and with a small dissipation $1/\omega_p\tau = 0.01$. We remark that while the nonlinear dipolium model [28] was developed for insulating materials, as it corresponds to a continuous distribution of small polarizable entities around which the electrons are localized, its results agree with those of a nonlinear hydrodynamical calculation [32] on a local *jellium* model of a conduction electronic fluid with a continuous electronic density profile at the surface. Thus, the results of the dipolium model may as well be applied to metals as to semiconductors and insulators as long as the results are written in terms of the linear dielectric response evaluated at the fundamental and SH frequencies. Note that there may be corrections arising from the spatial dispersion of the electron gas when the nonlocal character of the jellium model is incorporated [33]. In Fig. 3 we show the absolute values and phases of the nonlinear dipolar and quadrupolar response functions γ^d and γ^Q . Notice that both display very large resonant peaks corresponding to the surface plasmon resonance of the cylinder $\omega_{sp} = \omega_p/\sqrt{2}$ and to its subharmonic. Beyond abrupt changes at the

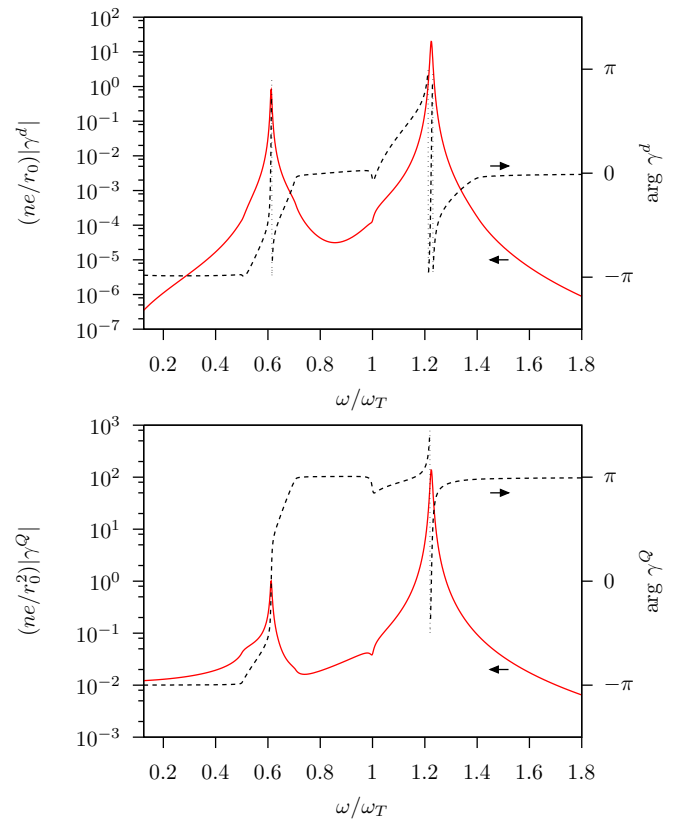


FIG. 4. Normalized absolute value (solid) and phase (dashed) of the dipolar (upper panel) and quadrupolar (lower panel) nonlinear response functions γ^d and γ^Q for a cylinder made of a dispersive dielectric with a Lorentzian resonance characterized by a longitudinal ω_L and a transverse ω_T frequency with $\omega_L = \sqrt{2}\omega_T$, a lifetime $\tau = 100/\omega_T$, and a deformation parameter $d = 0.01$, as a function of the normalized frequency ω/ω_T . The irrelevant abrupt 2π phase jumps are indicated with dotted vertical lines.

resonances, the phase of γ^d shifts away from 0 in a wide region that spans from $\omega_p/2$ up to ω_p . This is due to the logarithm term in Eq. (20), whose argument changes sign as ω or 2ω sweeps across the plasma frequency [28]. The phase of γ^Q also displays a smooth variation of around 2π in the same region.

In Fig. 4 we show the absolute values and phases of γ^d and γ^Q for a similar deformed cylinder but made up of an insulator. We assume its dielectric function is dispersive, and for simplicity we assume it has a single resonance described by a simple Lorentzian [31] form given by $\epsilon(\omega) = (\omega_L^2 - \omega^2 - i\omega/\tau)/(\omega_T^2 - \omega^2 - i\omega/\tau)$, where ω_L and ω_T are the frequencies of the longitudinal and transverse optical modes, respectively, and we included a small dissipation characterized by τ . For definitiveness, we took $\omega_L = \sqrt{2}\omega_T$ and $\omega_T\tau = 100$. Both γ^d and γ^Q show strong resonant peaks corresponding to the excitation of the surface plasmon-polariton at $\omega = \omega_{spp} = \omega_T\sqrt{3}/2$ and its subharmonic. The dielectric function crosses zero at ω_L and has a pole at $\omega_T = 1$. The phase of both γ^d and γ^Q grows smoothly between $\omega_T/2$ and $\omega_L/2$, and between ω_T and ω_L , save for abrupt jumps at $\omega_{spp}/2$, ω_T , and ω_{spp} , and it remains constant otherwise. Some features in the phase of γ^d and γ^Q are inherited from

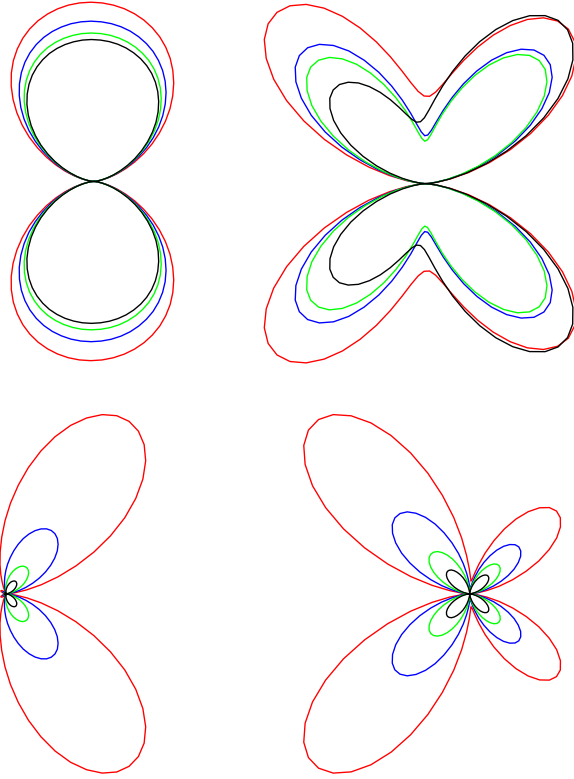


FIG. 5. Angular radiation pattern for a deformed metallic cylinder with deformation parameter $d = 0.01$ described by a Drude response for frequencies ω approaching ω_{sp} or to its subharmonic: $\omega < \omega_{sp}/2$ (upper left), $\omega_{sp}/2 < \omega$ (upper right), $\omega < \omega_{sp}$ (bottom left), and $\omega > \omega_{sp}$ (bottom right). As ω approaches a resonance, the total radiated power increases.

those of the parameter [28] a . We remark that close to a simple resonance, a Lorentzian response displays a rapid change of phase of π due to the change of sign of its real part across a pole. For a double or triple resonance, the corresponding change in phase would be 2π or 3π . We note that in our expressions for γ^d and γ^Q [Eqs. (30) and (31)] there are different terms displaying resonances of order 1, 2, and 3 and hence the total phase across a resonance depends on the competition between them. A logarithmic contribution to the phase is also present due to the existence of the parameter a in some terms. The above leads to distinct changes of the phase across the different resonance peaks in Figs. 3 and 4, with a magnitude that depends on which term was dominant. On the other hand, the vertical -2π abrupt jumps are irrelevant as they arise trivially from the fact that the phase is defined modulo 2π .

In Fig. 5 we plot the pattern $dP/d\theta$ versus the polar angle θ corresponding to a deformed metallic cylinder as that in Fig. 3, described by the Drude response and with a deformation parameter $d = 0.01$, illuminated by a TM electromagnetic wave propagating along the y axis with an electric field pointing along the x axis, assuming that the nominal radius $r_0 = c/4\omega_p$ of the cylinder is small compared to the wavelength, so we may assume the incoming field to be constant within the particle and use the expressions obtained in the previous section corresponding to a homogeneous ex-

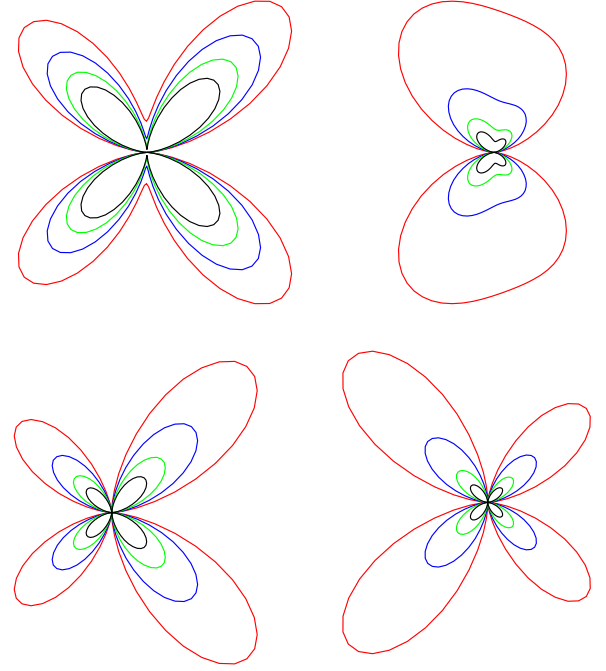


FIG. 6. Angular radiation pattern for a deformed dielectric cylinder with deformation parameter $d = 0.01$ described by a simple Lorentzian response with negligible dissipation for frequencies ω close to ω_{spp} or its subharmonic: $\omega < \omega_{spp}/2$ (upper left), $\omega_{spp}/2 < \omega$ (upper right), $\omega < \omega_{spp}$ (bottom left), and $\omega > \omega_{spp}$ (bottom right). As ω approaches a resonance, the total radiated power increases.

ternal field. Notice there is a competition between the dipolar and quadrupolar contributions to the radiation, and that their relative strength varies as the frequency increases. We remark that the SH dipole would be zero for the nondeformed cylinder, but for deformations as small as 1% its contribution to the radiation is comparable to the quadrupolar contribution. Figure 5 shows that for low frequencies, $\omega < \omega_{sp}/2$ displayed in the top left panel, the radiation is completely dominated by the dipolar term, and it displays the typical pattern consisting of two symmetrical lobes. As the frequency moves toward the resonance the total radiated power increases, hence the outermost curve in the top left panel corresponds to a frequency slightly below the resonance at $\omega_{sp}/2$. For higher frequencies the pattern becomes largely quadrupolar. The top right panel corresponds to $\omega > \omega_{sp}/2$ for which the quadrupolar contribution overshadows the dipolar contribution and a four-lobed pattern emerges. It is somewhat asymmetrical due to the interference with the dipolar field. Also note the shift in the size of the lobes from front to back as one moves away from the resonance at $\omega_{sp}/2$. The bottom left panel illustrates the radiation pattern for frequencies approaching ω_{sp} from below and is predominantly dipolar with an influence of the quadrupolar contribution, which makes it asymmetrical. Radiation at frequencies above that of the surface plasmon $\omega > \omega_{sp}$ is shown in the bottom right panel. In this region too, the pattern is mostly quadrupolar displaying four lobes that are asymmetrical due to the interference with the dipolar contribution to the radiation.

In Fig. 6 we show the SH angular radiation pattern as in Fig. 5 but corresponding to a dielectric particle as in Fig. 4.

Here, we also see the competition between the dipolar and the quadrupolar radiation with the variation in frequency and the asymmetry in the different lobes of the quadrupolar pattern arising due to the phase difference between the two terms. Similar to Fig. 5, as the frequency approaches a resonance the total radiated power increases. However, the quadrupolar contribution to the radiation is stronger at lower frequencies in this case, unlike the metallic case (Fig. 5). In the top left panel, we plot the patterns for $\omega < \omega_{\text{spp}}/2$ where the quadrupolar contribution to the radiation dominates the dipolar one and is therefore almost symmetric. The top right panel illustrates the radiation for frequencies $\omega > \omega_{\text{spp}}/2$. The outermost curve, closest and slightly above the resonance at $\omega_{\text{spp}}/2$, displays a slightly distorted dipolar pattern. Moving away from the resonance, the quadrupolar term gets relatively stronger and the competition between the two terms gives rise to an asymmetry in the pattern. The bottom left panel shows the pattern for $\omega < \omega_{\text{spp}}$, and it shows asymmetrical quadrupolar patterns with the asymmetry appearing in the outermost curves, just below the resonance frequency. The bottom right panel shows the radiation at higher frequencies $\omega > \omega_{\text{spp}}$, which is also symmetric and almost pure quadrupolar-like radiation.

We remark that our calculation above is strictly in 2D, while experimental realizations would most certainly be 3D, and we expect any nanowire to be of finite length. Nevertheless, our results may still be partially applicable for finite cylinders. Our calculation of the dipolar and quadrupolar nonlinear hyperpolarizabilities will hold true as long as the length l of the finite cylindrical nanowire is much larger than its nominal radius r_0 , a condition that is mostly obeyed in the experimental realization of nanowires. The 2D electromagnetic radiation in the plane of the cross section of the infinite cylinder was obtained in the radiation zone, where we assumed the distance r to the axis of the cylinder to be much larger than the wavelength. However, it must hold that this distance is smaller than the length of the cylinder. Thus, our calculated patterns would only be observable where $r_0 \ll \lambda$, $\lambda \ll r \ll l$ and only if both conditions may be satisfied together. Farther away, the 3D nature of the radiation pattern ought to be accounted for, and it might be calculated using antenna theory. Nevertheless, we emphasize that we expect that the *relative* magnitude between the dipolar and quadrupolar contributions to the radiation will remain as calculated above. A discussion of the effect of the finite length of the cylinder can be found in the work by Dadap [15].

IV. CONCLUSIONS

We developed an analytical formalism to study the second-order nonlinear optical response of isolated particles made of centrosymmetric materials with a cross section slightly deformed away from that of a centrosymmetric particle. To this end, we chose the most simple geometry that lacks inversion symmetry, namely a cylinder with an almost circular cross section with three small protuberances separated by an angle of $2\pi/3$. We employed a perturbative approach choosing the extent of the deformation away from the symmetrical geometry as the smallness parameter. This allowed us to obtain simple closed-form expressions for the electric fields

within and beyond the particles and on their surfaces at both the fundamental and second harmonic (SH) frequencies. The self-consistent field near the surface of the particle was used to calculate the induced nonlinear polarization employing the results of the dipolium model [28]. Within the framework of that model, the nonlinear response of the surface is only due to the abrupt variations of the electric field across its selvedge, and the bulk and surface response are determined completely by the linear dielectric function of the material evaluated at the fundamental and second harmonic frequencies. Thus, intrinsic surface effects, such as those due to transitions to and from the surface states, surface reconstructions, and relaxation, are neglected. Local field effects and crystal structure have also been ignored in the model. Hence, we must point out that we expect our calculation to fail to describe spectral features arising from such effects. However, the comparison of our calculation with experimental results may allow us to identify the strength of those contributions we left out.

The induced nonlinear polarization was used to calculate the self-consistent SH fields and the nonlinear hyperpolarizabilities. The zeroth-order term in their expansion in powers of the deformation parameter corresponds to the case of a symmetric cylinder yielding no SH dipole but a nonzero quadrupolar response. At the first order in the deformation, the effect of a small deviation from centrosymmetric geometry yields a dipolar contribution proportional to the deformation parameter, which increases with the size of deformation and competes with that of the quadrupole already for very slightly deformed metallic and dielectric particles. We have only considered the dominant dipolar and quadrupolar contributions to the nonlinear hyperpolarizabilities in this work, as the higher-order multipoles generate a much weaker SH signal.

The dipolar and quadrupolar nonlinear responses were obtained in terms of the linear dielectric response of the material at the fundamental and SH frequencies and were found to have resonant structures corresponding to the poles and zeros of the dielectric function, and to the surface plasmon or surface plasmon-polariton frequencies of the undeformed particle, and to their subharmonics, as well as additional structure due to the normal nonlinear surface parameter a . We showed results for particles made up of a Drude metal and of a dielectric characterized by a simple Lorentzian response, as they allow a simple interpretation of the resulting spectra and radiation patterns. Nevertheless, as the input to our calculations is the dielectric functions of the particles, they may be applied to particles made of arbitrary materials for which ϵ is known. Our approach can also be generalized to other geometries. Finally, we showed that the dipolar SH radiation is comparable and may overshadow the quadrupolar contribution for deformations as small as 1%. On the other hand, at resonance, the dipolar hyperpolarizabilities (per unit length) reached values several orders of magnitude larger than r_0/ne , with r_0 the nominal size of the particle, n the polarizable entity or the electronic number density, and e the electronic charge (see Figs. 3 and 4). Thus, we expect that the dipolar nonlinear susceptibility of a metamaterial made up of these particles could be much larger than $1/ner_0$. As the typical susceptibility of noncentrosymmetric materials is of order $1/nea_B$ with a_B the Bohr's radius, a metamaterial made of centrosymmetric

materials with a noncentrosymmetric geometry may be a competitive source of SH provided a_B/r_0 is not too small. Finally, we remark that our calculation of the nonlinear response of a particle showed that there are some subtleties to be accounted for: bulk contributions, bulk induced surface charges, surface originated surface charges, and surface dipolar layers. All of these have to be appropriately screened to get consistent expressions for the hyperpolarizabilities. Analytical results for simple models that take all of these contributions into account are important in order to calibrate and test numerical calculations, which may then, if proven to be correct, be applied to a larger class of systems. We expect that the present results will be useful for this purpose.

ACKNOWLEDGMENTS

This work was supported by DGAPA, UNAM under Grants No. IN113016 and No. IN111119 (WLM) and by CONACyT (R.S.). We acknowledge useful talks with V. Agarwal, A. Reyes-Esqueda, L. Juárez-Reyes, and B. S. Mendoza.

APPENDIX

In this Appendix, we calculate the fields in the radiation zone due to localized systems of oscillating charge and current densities in 2D in order to obtain the corresponding angular radiation patterns. We will only consider electric dipole and quadrupole radiation. The treatment is predominantly similar to that of 3D [27], but using the Green's function for the 2D wave equation, and we follow Ref. [34].

We will consider a harmonically varying monochromatic current distribution $\mathbf{J}(\mathbf{r}, t) = \mathbf{J}(\mathbf{r})e^{-i\omega t}$. In the Lorentz gauge, the vector potential is also monochromatic and obeys a wave equation that becomes a Helmholtz equation for its amplitude $\mathbf{A}(\mathbf{r})$ with a source $-4\pi\mathbf{J}(\mathbf{r})/c$. To solve it, we first find the corresponding Green's function in 2D $G(|\mathbf{r} - \mathbf{r}'|)$, which obeys

$$(\nabla^2 + k^2)G(r) = -4\pi\delta(\mathbf{r}). \quad (\text{A1})$$

Beyond the singularity, $G(r) = R(kr)$, where

$$s^2 \frac{d^2}{ds^2} R(s) + s \frac{d}{ds} R(s) + s^2 R(s) = 0. \quad (\text{A2})$$

The solution is proportional to an outgoing Hankel function $H_0^{(1)}(s)$, which in the near zone, ($s \rightarrow 0$), takes the form

$$\lim_{s \rightarrow 0} H_0^{(1)}(s) = 2i \ln(s)/\pi. \quad (\text{A3})$$

As the nonretarded Green's function in 2D is $G = -2 \ln(r) + \text{const}$, a comparison with Eq. (A3) yields $G(r) = i\pi H_0^{(1)}(kr)$. Thus, using the asymptotic expression for Hankel's function for large arguments, we obtain in the radiation zone ($kr \rightarrow \infty$),

$$G(r) = e^{i\pi/4} \sqrt{\frac{2\pi}{kr}} e^{ikr}. \quad (\text{A4})$$

The retarded vector potential is then

$$\mathbf{A}(\mathbf{r}) = \frac{1}{c} \int d^2r' e^{i\pi/4} \sqrt{\frac{2\pi}{k|\mathbf{r} - \mathbf{r}'|}} e^{ik|\mathbf{r} - \mathbf{r}'|} \mathbf{J}(\mathbf{r}'). \quad (\text{A5})$$

For a localized source in the long-wavelength approximation $r' \ll \lambda \ll r$ one can approximate Eq. (A5) as

$$\mathbf{A}(\mathbf{r}) \approx \frac{1}{c} \sqrt{\frac{2\pi}{kr}} e^{i\pi/4} e^{ikr} \int d^2r' \mathbf{J}(\mathbf{r}') \sum_{m=0} \frac{(-ik)^m}{m!} (\hat{\mathbf{r}} \cdot \mathbf{r}')^m. \quad (\text{A6})$$

The first term ($m = 0$) in the series (A6) may be integrated to obtain the dipolar contribution to the potential,

$$\mathbf{A}^{(0)} = (-ie^{i\pi/4}) \sqrt{2\pi} \sqrt{\frac{k}{r}} e^{ikr} \mathbf{p}, \quad (\text{A7})$$

where \mathbf{p} is the amplitude of the oscillating dipole moment per unit length. The second term ($m = 1$) is

$$\mathbf{A}^{(1)}(\mathbf{r}) = \frac{1}{c} \sqrt{\frac{2\pi}{kr}} e^{i\pi/4} e^{ikr} (-ik) \int d^2r' \mathbf{J}(\mathbf{r}') (\hat{\mathbf{r}} \cdot \mathbf{r}'). \quad (\text{A8})$$

Within the integral, we can write $\mathbf{J}(\mathbf{r}') (\hat{\mathbf{r}} \cdot \mathbf{r}') = (1/2)\{\mathbf{J}(\mathbf{r}') (\hat{\mathbf{r}} \cdot \mathbf{r}') + \mathbf{r}' [\hat{\mathbf{r}} \cdot \mathbf{J}(\mathbf{r}')]\} + (1/2)\{\mathbf{J}(\mathbf{r}') (\hat{\mathbf{r}} \cdot \mathbf{r}') - \mathbf{r}' [\hat{\mathbf{r}} \cdot \mathbf{J}(\mathbf{r}')]\}$ as a sum of a symmetric and an antisymmetric part. The former can be manipulated to yield

$$\mathbf{A}^{(1s)}(\mathbf{r}) = (\sqrt{2\pi} e^{i\pi/4}) \frac{e^{ikr}}{4\sqrt{r}} k^{3/2} \mathbf{Q} \cdot \hat{\mathbf{r}}, \quad (\text{A9})$$

where \mathbf{Q} is the 2D quadrupolar tensor [Eq. (3)]. The antisymmetric part yields the magnetic dipolar radiation, which we ignore as in our system there is no magnetic dipole.

As usual, we may obtain the electromagnetic radiation field as $\mathbf{B} = \nabla \times \mathbf{A} \approx ik\hat{\mathbf{r}} \times \mathbf{A}$ and $\mathbf{E} = \mathbf{B} \times \hat{\mathbf{r}}$, so that from Eqs. (A7) and (A9) we obtain Eqs. (32) and (33).

-
- [1] D. Smirnova and Y. S. Kivshar, Multipolar nonlinear nanophotonics, *Optica* **3**, 1241 (2016).
 [2] Y.-x. Zhang and Y.-h. Wang, Nonlinear optical properties of metal nanoparticles: A review, *RSC Adv.* **7**, 45129 (2017).
 [3] V. L. Brudny, B. S. Mendoza, and W. L. Mochán, Second-harmonic generation from spherical particles, *Phys. Rev. B* **62**, 11152 (2000).
 [4] B. Huo, X. Wang, S. Chang, and M. Zeng, Second harmonic generation of a single centrosymmetric nanosphere illuminated

by tightly focused cylindrical vector beams, *J. Opt. Soc. Am. B* **29**, 1631 (2012).

- [5] J.-W. Sun, X.-H. Wang, S.-J. Chang, M. Zeng, and N. Zhang, Second harmonic generation of metal nanoparticles under tightly focused illumination, *Chin. Phys. B* **25**, 37803 (2016).
 [6] B. K. Canfield, H. Husu, J. Laukkanen, B. Bai, M. Kuittinen, J. Turunen, and M. Kauranen, Local field asymmetry drives second-harmonic generation in noncentrosymmetric nanodimers, *Nano Lett.* **7**, 1251 (2007).

- [7] S. Park, J. W. Hahn, and J. Y. Lee, Doubly resonant metallic nanostructure for high conversion efficiency of second harmonic generation, *Opt. Express* **20**, 4856 (2012).
- [8] J. Butet, G. Bachelier, I. Russier-Antoine, F. Bertorelle, A. Mosset, N. Lascoux, C. Jonin, E. Benichou, and P.-F. Brevet, Nonlinear Fano profiles in the optical second-harmonic generation from silver nanoparticles, *Phys. Rev. B* **86**, 075430 (2012).
- [9] R. Zhou, H. Lu, X. Liu, Y. Gong, and D. Mao, Second-harmonic generation from a periodic array of noncentrosymmetric nanoholes, *J. Opt. Soc. Am. B* **27**, 2405 (2010).
- [10] W. L. Schaich, Second harmonic generation by periodically structured metal surfaces, *Phys. Rev. B* **78**, 195416 (2008).
- [11] R. Czaplicki, J. Mäkitalo, R. Siikanen, H. Husu, J. Lehtolahti, M. Kuitinen, and M. Kauranen, Second-harmonic generation from metal nanoparticles: Resonance enhancement versus particle geometry, *Nano Lett.* **15**, 530 (2015).
- [12] J. I. Dadap, J. Shan, and T. F. Heinz, Theory of optical second-harmonic generation from a sphere of centrosymmetric material: Small-particle limit, *J. Opt. Soc. Am. B* **21**, 1328 (2004).
- [13] A. G. F. de Beer and S. Roke, Nonlinear Mie theory for second-harmonic and sum-frequency scattering, *Phys. Rev. B* **79**, 155420 (2009).
- [14] A. Capretti, C. Forestiere, L. Dal Negro, and G. Miano, Full-wave analytical solution of second-harmonic generation in metal nanospheres, *Plasmonics* **9**, 151 (2014).
- [15] J. I. Dadap, Optical second-harmonic scattering from cylindrical particles, *Phys. Rev. B* **78**, 205322 (2008).
- [16] C. I. Valencia, E. R. Méndez, and B. S. Mendoza, Second-harmonic generation in the scattering of light by two-dimensional particles, *J. Opt. Soc. Am. B* **20**, 2150 (2003).
- [17] C. I. Valencia, E. R. Méndez, and B. S. Mendoza, Second-harmonic generation in the scattering of light by an infinite cylinder, *J. Opt. Soc. Am. B* **21**, 36 (2004).
- [18] N. K. Balla, P. T. C. So, and C. J. R. Sheppard, Second harmonic scattering from small particles using discrete dipole approximation, *Opt. Express* **18**, 21603 (2010).
- [19] G. Bachelier, I. Russier-Antoine, E. Benichou, C. Jonin, and P.-F. Brevet, Multipolar second-harmonic generation in noble metal nanoparticles, *J. Opt. Soc. Am. B* **25**, 955 (2008).
- [20] J. Butet and O. J. F. Martin, Evaluation of the nonlinear response of plasmonic metasurfaces: Miller's rule, nonlinear effective susceptibility method, and full-wave computation, *J. Opt. Soc. Am. B* **33**, A8 (2016).
- [21] J. Butet, B. Gallinet, K. Thyagarajan, and O. J. F. Martin, Second-harmonic generation from periodic arrays of arbitrary shape plasmonic nanostructures: A surface integral approach, *J. Opt. Soc. Am. B* **30**, 2970 (2013).
- [22] C. Forestiere, A. Capretti, and G. Miano, Surface integral method for second harmonic generation in metal nanoparticles including both local-surface and nonlocal-bulk sources, *J. Opt. Soc. Am. B* **30**, 2355 (2013).
- [23] L. Zhang, S. Tao, Z. Fan, and R. Chen, Efficient method for evaluation of second-harmonic generation by surface integral equation, *Opt. Express* **25**, 28010 (2017).
- [24] G. D. Bernasconi, J. Butet, and O. J. F. Martin, Mode analysis of second-harmonic generation in plasmonic nanostructures, *J. Opt. Soc. Am. B* **33**, 768 (2016).
- [25] C. G. Biris and N. C. Panoiu, Second harmonic generation in metamaterials based on homogeneous centrosymmetric nanowires, *Phys. Rev. B* **81**, 195102 (2010).
- [26] U. R. Meza, B. S. Mendoza, and W. L. Mochán, Second-harmonic generation in nanostructured metamaterials, *Phys. Rev. B* **99**, 125408 (2019).
- [27] J. D. Jackson, *Classical Electrodynamics*, 2nd ed. (Wiley, New York, 1975).
- [28] B. S. Mendoza and W. L. Mochán, Exactly solvable model of surface second-harmonic generation, *Phys. Rev. B* **53**, 4999 (1996).
- [29] J. Rudnick and E. A. Stern, Second-harmonic radiation from metal surfaces, *Phys. Rev. B* **4**, 4274 (1971).
- [30] M. W. Klein, M. Wegener, N. Feth, and S. Linden, Experiments on second- and third-harmonic generation from magnetic metamaterials, *Opt. Express* **15**, 5238 (2007).
- [31] N. Ashcroft and N. Mermin, *Solid State Physics* (Saunders College, Philadelphia, 1976).
- [32] J. A. Maytorena, B. S. Mendoza, and W. L. Mochán, Theory of surface sum frequency generation spectroscopy, *Phys. Rev. B* **57**, 2569 (1998).
- [33] J. A. Maytorena, W. L. Mochán, and B. S. Mendoza, Hydrodynamic model for SHG at conductor surfaces with continuous profiles, *Phys. Rev. B* **51**, 2556 (1995).
- [34] R. Singla and W. L. Mochán (unpublished).